Rev. Roum. Sci. Techn.– Électrotechn. et Énerg.
Vol. **66**, *2*, pp. 77–83, Bucarest, 2021

MECHANICAL SENSOR FAULT-TOLERANT CONTROLLER IN PMSM DRIVE: EXPERIMENTAL EVALUATION OF OBSERVERS AND SIGNAL INJECTION FOR POSITION ESTIMATION

SLIMANE MEDJMADJ[1], DEMBA DIALLO[2], ANTONI ARIAS[3]

Key words: Permanent-Magnet Synchronous Motor, Sensorless Control, Fault Tolerant Control (FTC), High Frequency Injection, Kalman Filter.

This paper presents the operating principle, results and conclusions for an FTC mechanical sensor that can guarantee continuity of operation on the whole speed range. This active FTC is based on analytical redundancy using three different estimators (an Extended Kalman Filter (EKF), a back electromotive force based observer (back-EMF observer) and a high frequency voltage injection (HFI). Thanks to this structure, the mechanical measurement is continuously monitored and at sensor fault occurrence the sensorless controller can be engaged using the best estimate. From numerical simulations and experimental results on a 1.1kW salient PMSM drive, the following conclusion has been drawn : at low and zero speed, the drive availability is obtained with the combination of the EKF and the HFI while for higher speeds EKF and back-EMF observer have better performance.

NOMENCLATURE

L_d, L_q are the direct and quadratic stator inductances,
R_s is the stator resistance,
Ψ_m is the magnetic flux linkage,
p is the number of pole pairs,
Ω is the rotor mechanical speed, Ω_V is the output of the voting algorithm,
$\omega = p\Omega$ is the electrical angular velocity,
θ is the electrical rotor position, θ_V is the output of the voting algorithm,
x, a variable, $\hat{x}$ is the estimated variable, x^t is the transpose,
x_α, x_β are the components of x in the (α,β) reference frame,
x_d, x_q are the components of x in the (d,q) reference frame.
Parameters of the high frequency sinusoidal injected voltage:
ω_i is the frequency, V_{si} is the amplitude,
$\hat{e}_{s\alpha}$, $\hat{e}_{s\beta}$ are the back-electromotive-force estimates in the (α,β) reference frame,
$\hat{\hat{e}}_{s\alpha}$, $\hat{\hat{e}}_{s\beta}$ are the outputs of the adaptive observer.

1. INTRODUCTION

Because of its attractive features, like high efficiency, high power density, ease of control and high power/torque density, Permanent Magnet Synchronous Motors (PMSM) are increasingly used in many industrial applications. For transportation (ground or aircraft) continuous operation is necessary and thus even a breakdown of the drive is unacceptable [1]. However different faults or failures can affect the drive (electrical machine, power converter(s), cables, energy sources or sensors) [2]. The resilience of the drive can be obtained:

- through a conservative design or/and,
- a fault tolerant controller [3–5].

In the first case, hardware redundancy is implemented with for example additional windings for the electrical machine, additional legs for the power converter and additional sensors.

This solution even unavoidable in some sensitive applications may be expensive and may require specific layout as the accessibility of the machine neutral point or the direct current power supply midpoint.

The other option is to design a controller that can cope with the faults or failures and make the drive resilient. The so-called fault tolerant controller (FTC) can be passive (meaning that there is no fault diagnosis module and the resilience is based on robust controllers) or active (there is a Fault Detection and Isolation module and a supervision module). In the active FTC, analytical redundancy is used to estimate information that may be lost or degraded. This is the case for the mechanical sensor for example. In fact, an accurate rotor position sensor (encoder, resolver, Hall-effect sensor, etc.) is required to achieve rotor position/speed/torque control. In case of faulty sensor, the information must be recovered from the available electrical measurements, the drive becomes by abuse of language sensorless [6–7]. In general, there are three different approaches:

- the estimation of the motor back electromotive forces (EMF) [8];
- state estimation with differential algebraic [9] or linear/non-linear observers (backstepping, Luenberger, fuzzy sliding mode and Kalman filter [10–12]);
- inject a high frequency additional voltage at the machine terminals and retrieve the rotor position from current signal processing [13–15].

These three methods do not have the same static and dynamic performances on the whole speed range. Therefore, it sounds relevant to evaluate a hybrid solution with the three methods and the actual sensor in a FTC architecture to ensure the continuity of operation with an effective and robust FTC.

Compared to the works previously mentioned, fault-tolerant control (FTC) has been proposed especially for low, very low or only for middle and high-speed ranges. However, FTC over the entire speed range has not been largely studied. This paper brings a contribution with a

[1] Laboratory of Control Univ.of Setif and university of Bordj Bou Arreridj, Algeria, s.medjmadj@univ-bba.dz
[2] Uinversité Paris-Saclay, CentraleSupélec, CNRS, Group of Electrical Engineering Paris, Sorbonne Université, 91192 Gif Sur Yvette, France, demba.diallo@geeps.centralesupelec.fr
[3] UPC, Barcelona, Spain, antoni.arias@upc.edu.

proposal of a FTC on the whole speed range. The proposed hybrid structure has the capability of mechanical sensor fault detection, fault isolation, and reconfiguration over the entire speed range.

The paper is divided in four sections. Section 2 is dedicated to the description of the three estimators and the evaluation of their performances within the FTC structure through numerical simulation results. Section 3 presents the evaluation of the three estimators with experimental results. Finally, a conclusion closes the paper.

2. FAULT-TOLERANT CONTROL STRUCTURE

2.1. POSITION/ SPEED ESTIMATORS

This section presents the three different methods for speed and position estimations in sensorless control of PMSM.

A. EXTENDED KALMAN FILTER (EKF)

The electrical equations of a PMSM in the standard (*d,q*) synchronous rotating reference frame are shown as follows:

$$\frac{\mathrm{d}X(t)}{\mathrm{d}t} = A_c(\Theta)X(t) + B_c''(\Theta)U(t)B_c^{\Theta}(\Theta)\Theta(t), \qquad (1)$$

where

$$A_c(\Theta) = \begin{bmatrix} -\frac{R_s}{L_d} & \frac{\omega L_q}{L_d} \\ -\frac{\omega L_d}{L_q} & -\frac{R_s}{L_q} \end{bmatrix} \; ; \; B_c^u(\Theta) = \begin{bmatrix} \frac{\cos\theta}{L_d} & \frac{\sin\theta}{L_d} \\ -\frac{\sin\theta}{L_q} & \frac{\cos\theta}{L_q} \end{bmatrix}$$

$$B_c^{\Theta} = \begin{bmatrix} 0 & 0 \\ -\frac{\Psi_m}{L_q} & 0 \end{bmatrix} \quad ; \quad C(\Theta) = \begin{bmatrix} \cos\theta & -\sin\theta \\ \sin\theta & \cos\theta \end{bmatrix}$$

where, $v_{s\alpha,s\beta}$ and $i_{s\alpha,s\beta}$ are the stator voltage and current, respectively in the stationary reference frame (α,β). $i_{sd,\,sq}$ are the currents in rotating (*d,q*) synchronous frame. Using the current measurements $(i_{s\alpha}, i_{s\beta})$ and the controller-output voltages $(v_{s\alpha}, v_{s\beta})$ and the digitalized model in (1), the EKF can be designed as detailed in [7–8], [16–18].

B. BACK-EMF OBSERVER

A state representation in the (αβ) coordinates of the salient PMSM is modelled as [6]:

$$\frac{d}{dt}\begin{bmatrix} i_{s\alpha} \\ i_{s\beta} \end{bmatrix} = \frac{1}{L_d}\begin{bmatrix} -R_s & -w(L_d - L_q) \\ w(L_d - L_q) & -R_s \end{bmatrix}\begin{bmatrix} i_{s\alpha} \\ i_{s\beta} \end{bmatrix} + \frac{1}{L_d}\begin{bmatrix} -1 & 0 \\ 0 & -1 \end{bmatrix}\begin{bmatrix} e_{s\alpha} \\ e_{s\beta} \end{bmatrix} + \frac{1}{L_d}\begin{bmatrix} v_{s\alpha} \\ v_{s\beta} \end{bmatrix} \qquad (2)$$

where $e_{s\alpha}, e_{s\beta}$ are the Back-EMF in the (α,β) coordinates. They are defined as:

$$\begin{bmatrix} e_{s\alpha} \\ e_{s\beta} \end{bmatrix} = \left[(L_d - L_q)(w i_{sd} - \frac{di_{sq}}{dt}) + \Psi_m w\right]\begin{bmatrix} -\sin\theta \\ \cos\theta \end{bmatrix}, \qquad (3)$$

where G is a positive gain tuned with pole-placement technique of the adaptive observer obtained after the development [18]

$$\begin{aligned} \dot{\hat{e}}_{s\alpha} &= -\hat{w}\,\hat{e}_{s\beta} - G\left(\hat{e}_{s\alpha} - \hat{e}_{s\alpha}\right) \\ \dot{\hat{e}}_{s\beta} &= -\hat{w}\,\hat{e}_{s\alpha} - G\left(\hat{e}_{s\beta} - \hat{e}_{s\beta}\right) \end{aligned}. \qquad (4)$$

The error dynamics are given as:

$$\begin{aligned} \dot{\tilde{e}}_{s\alpha} &= -\tilde{w}\,\hat{e}_{s\beta} - G\tilde{e}_{s\alpha} \\ \dot{\tilde{e}}_{s\beta} &= \tilde{w}\,\hat{e}_{s\alpha} - G\tilde{e}_{s\beta} \end{aligned}. \qquad (5)$$

Concerning the Back-EMF adaptive observer for PMSM, more details can be found in [19–21].

C. HIGH FREQUENCY SIGNAL INJECTION ESTIMATOR

Thanks to the PMSM magnetic saliency, the inductances in the d and q axes are not constant and depend on the rotor position. If beside the fundamental component, an additional sinusoidal voltage is injected at the machine terminals, there will be an additional component in the currents flowing in the windings. If the additional voltage frequency is high enough, the rotor position can be deduced from the spectral processing of this new current component that does not produce a parasitic torque [22]. The methodology to select the appropriate high-frequency signal injection voltage amplitude for rotor position estimation is described in [13].

The injection frequency f_i (set hereafter at 1 kHz) is ten times higher than the fundamental frequency. In this work we consider a rotating HF voltage signal as an additional signal. It is a balanced three-phase voltage set with constant amplitude V_{si} rotating at the frequency $\omega_i = 2\pi f_i$, which becomes in a two-axis stationary reference frame:

$$\begin{bmatrix} V_{\alpha i} \\ V_{\beta i} \end{bmatrix} = V_{si}\begin{bmatrix} -\sin(\omega_i t) \\ \cos(\omega_i t) \end{bmatrix}. \qquad (6)$$

The *dq* PMSM can be modeled in the rotor reference frame by the following set of equations:

$$\begin{cases} V_d = R_s i_d + \rho\Psi_d - w_r\Psi_q \\ V_q = R_s i_q + w_r\Psi_d + \rho\Psi_q \end{cases}, \qquad (7)$$

where ρ is a differential operator. The flux linkage vector is:

$$\begin{cases} \Psi_d = L_d i_d + \Psi_m \\ \Psi_q = L_q i_q \end{cases}. \qquad (8)$$

Transforming (7) into the (α,β) where w_r = 0, the following voltage relation is obtained:

$$\begin{cases} V_\alpha = R_s i_\alpha + \rho\Psi_\alpha \\ V_\beta = R_s i_\beta + \rho\Psi_\beta \end{cases} \qquad (9)$$

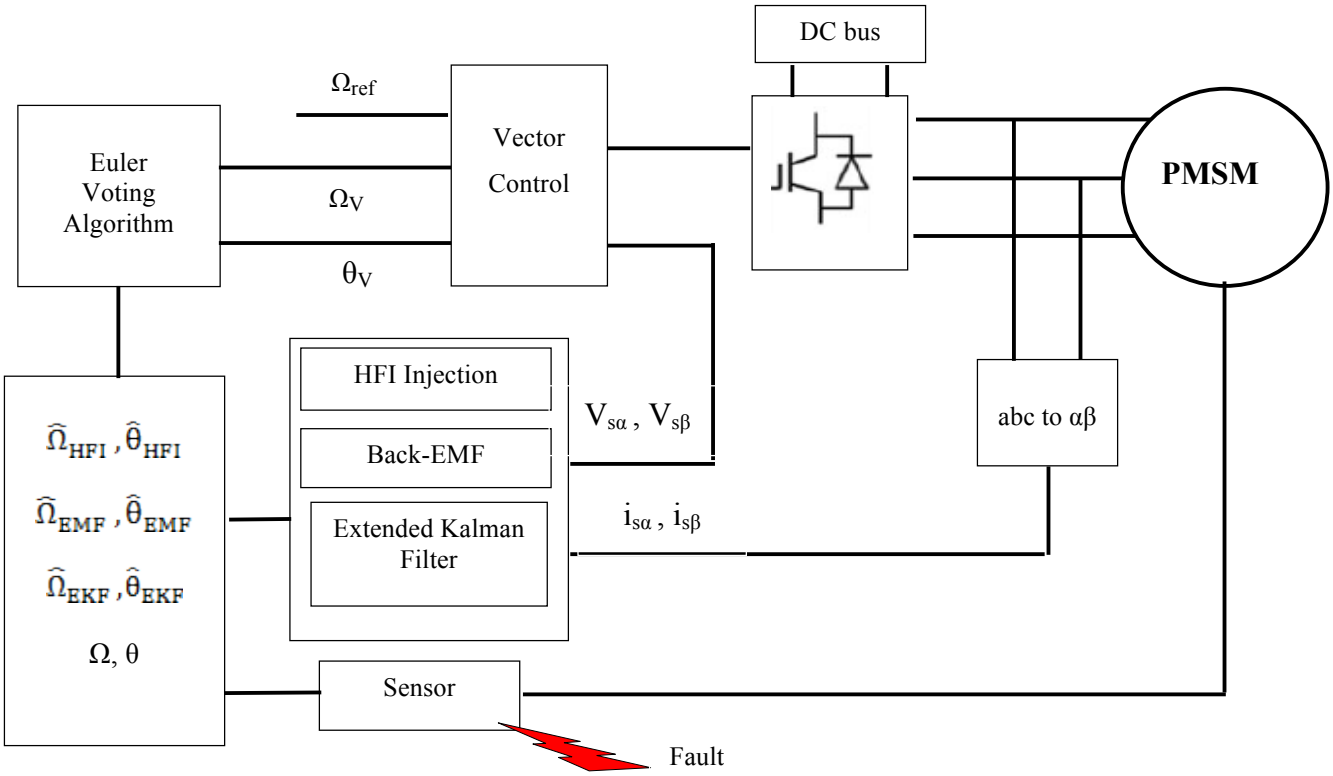

Fig. 1 – Position sensor fault tolerant controller PMSM drive.

If the resistance R_s is neglected at high frequency the currents can be deduced from the following expressions [13,23,24]:

$$\begin{bmatrix} i_{\alpha i} \\ i_{\beta i} \end{bmatrix} = \begin{bmatrix} I_{i0}\cos(\omega_i t) + I_{i1}\cos(2\theta - \omega_i t) \\ I_{i0}\sin(\omega_i t) + I_{i1}\sin(2\theta - \omega_i t) \end{bmatrix}, \quad (10)$$

with

$$I_{i0} = \frac{V_{si}(L_q + L_d)}{2\omega_i L_q L_d}; \quad I_{i1} = \frac{V_{si}(L_q - L_d)}{2\omega_i L_q L_d}.$$

Equation (10) contains information on the rotor position 2θ [24,25], that can be estimated with the arctangent function

$$\hat{\theta} = \frac{1}{2}\arctan\left(\frac{i_\beta}{i_\alpha}\right). \quad (11)$$

2.2. SENSOR FAULT-TOLERANT CONTROL MECHANISM

The objective of a fault tolerant controller is to guarantee that the process is under control even in case of fault or failure before the intervention of the maintenance team [26]. There are two main FTC approaches: passive and active [27–31]. In the following an active FTC is investigated as displayed in Fig. 1.

In healthy condition, the sensor gives the mechanical information. However, when a fault arises, an estimated position is computed by each of the three estimators. A voting algorithm based on Euler method is then used to select the most relevant information for feedback (denoted Ωv, θv respectively for the mechanical speed and the electrical position). The threshold has been set after numerous simulations on the whole torque-speed range and the computation of the errors between the output of the sensor and the estimates. The transient behavior of the observers has been analyzed by the Euler method for its good dynamic performances, robustness to parametric variations, simplicity of implementation and tuning. The monitoring of the sensor requires comparing its output with at least two other measurements or estimates. Thus, it is possible to detect the sensor fault. However, as mentioned above, the three approaches do not have the same static and dynamic performances over the entire speed range. The flowchart of the Euler method is shown in Fig. 2.

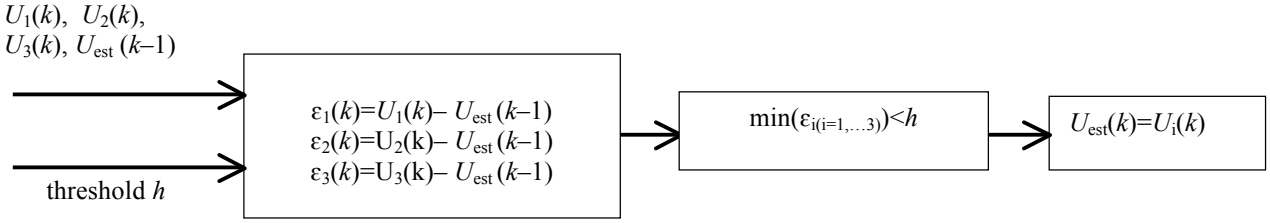

Fig. 2 – Flowchart of the voting algorithm with Euler for k^{th} sampling time.

2.3 SIMULATION RESULTS OF THE FTC

To evaluate the performances of the estimators and the FTC, a set of simulations has been performed using Matlab/Simulink. The PMSM, whose parameters are shown in Table I, is fed with a PWM voltage source inverter. The current control loop is sampled at 100 µs while the speed loop sampling frequency is 1 kHz.

To evaluate the FTC, the following scenario is used:

- a time varying speed reference from 0 to 10 at 100 rad/s,
- a load torque of 2.5 Nm (75% of the nominal load torque) is applied in the following time ranges in second [1.5 – 2], [4 – 4.5] and [7 – 7.5].

A mechanical sensor failure (complete outage) is introduced in steady states (at low and high speed) and during a speed transient. Figure 3a displays in solid line the actual measured mechanical speed (Ω+fault) and in dashed lines the speed selected by the voting algorithm from the three estimators. Figure 3b shows the transformed currents I_d and I_q.

Table 1

PMSM Parameters

Parameter	Value
Magnetic flux (Ψm)	0.153 Wb
Nominal speed (Ωn)	314 rad/s
Nominal load torque (*T*n)	3.2 Nm
d-axis inductance (*L*d)	3.5 mH
q-axis inductance (*L*q)	4.5 mH
Stator resistance (*R*s)	1.65 Ω
Moment of inertia (*J*)	6.4 10-3 kg/m²
Viscous friction (*F*)	509 10 -3 Nm/rad
Pole pairs (*p*)	3
Nominal voltage (*V*n)	200 V
Nominal current (*I*n)	6 A

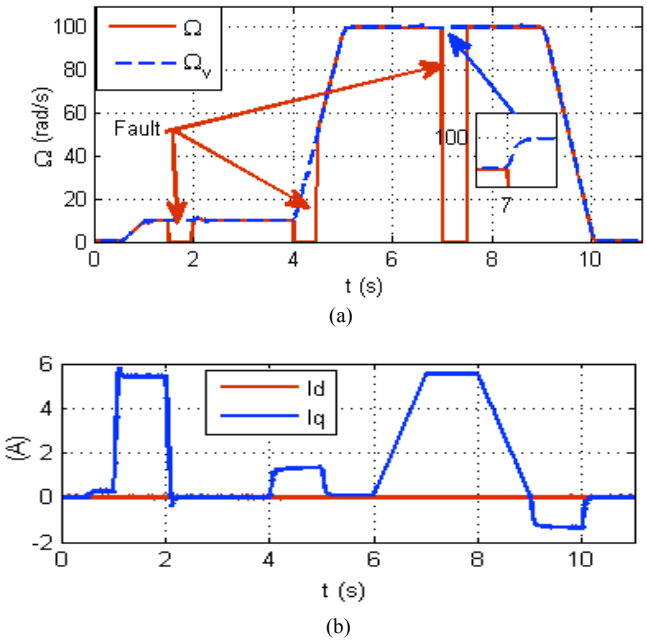

(a)

(b)

Fig. 3 – Fault tolerant control under sensor failure and recovery.

Figure 4a shows the operation of the voting algorithm. It can be noticed that in low speed, the HFI estimator is selected while as the speed increases the Back-EMF observer is preferred. The curves plotted in Fig. 4b represent the errors between the output of the voting algorithm and the outputs of the estimators. In the following, the robustness of the FTC is evaluated against parameter variation.

With +50 % variation introduced in the stator resistance Rs, the simulation results displayed in figure 5 show that the FTC is still efficient.

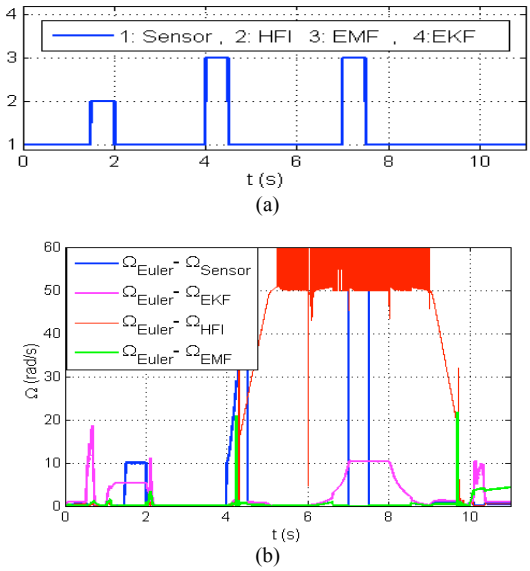

(a)

(b)

Fig. 4 – Operation of the voting algorithm.

According to the previous simulation results, we can conclude:

1. The HFI estimator is efficient in the low-speed operation meaning from zero to 10% of the nominal speed (Ωn)
2. The back-EMF observer is efficient for higher speeds (Ω >10 % Ωn).

We can also retrieve from the results in the literature [17] that the EKF is efficient on the whole speed range despite the computational burden if the gains are computed online.

In conclusion, to guarantee the continuity of operation in the whole speed range, the voting algorithm must always have three inputs to discriminate a faulty mechanical sensor. Therefore, the FTC will be based on the appropriate selection of estimators depending on the speed as displayed in Fig. 6.

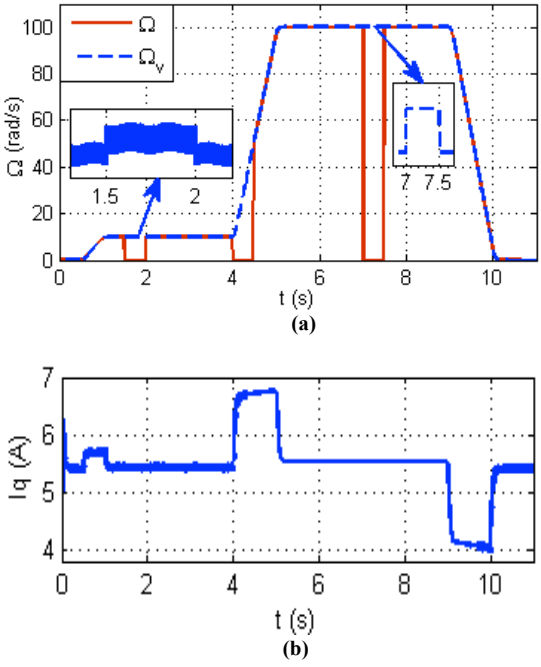

(a)

(b)

Fig. 5 – Fault tolerant control under Rs variation (+50 %).

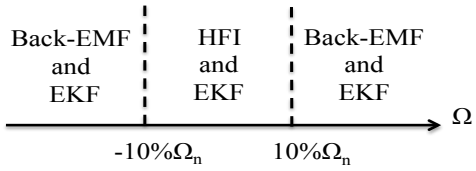

Fig. 6 – Combination of estimators on the whole speed range.

3. EXPERIMENTAL RESULTS AND EVALUATION OF THE ESTIMATORS

The experiments are run on the 1.1kW salient PMSM (as in Table I) drive. The PWM switching frequency of the inverter is 20 kHz, and the DC bus voltage is 200V. A dSpace 1103 RTI is used to implement all the algorithms at 10 kHz. The drive operating in sensorless mode means that one estimate is fed back to the vector control.

Fig. 7 – Experimental test bench.

In the following the drive operates in sensorless mode means that one estimate is fed back to the controllers and the transformations. Finally, the sensorless feasibility has been experimentally proven in case of an absolute encoder on the whole speed range.

The first operating point is at low speed (the speed reference varies from +31.4 to −31.4 rad/s) and no load. The results are displayed in Figs. 8−10 respectively for the EKF, the Back-EMF and the HFI.

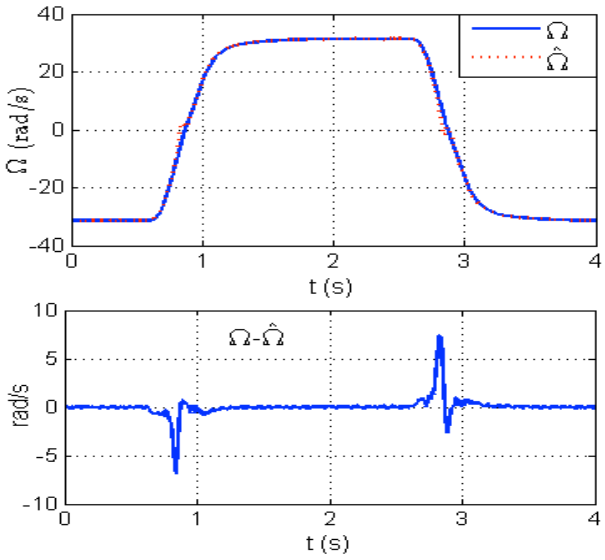

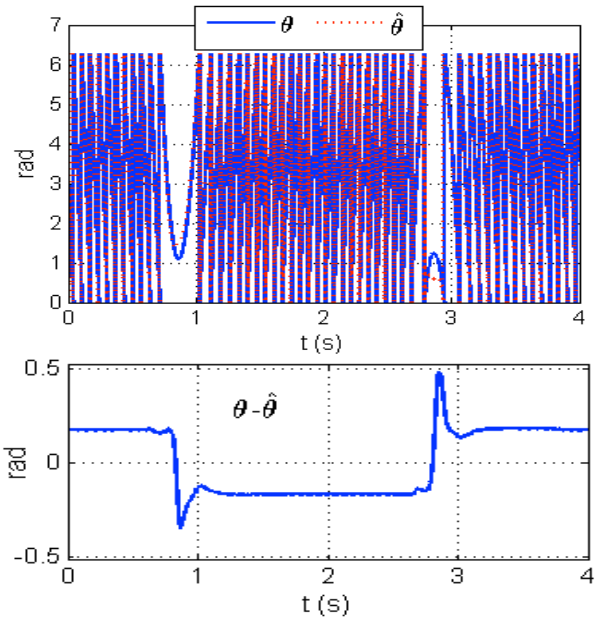

Fig. 8 – EKF Experimental results for speed and position estimations during a speed reversal test.

The electrical position estimation errors are inferior to ± 0.5 rad (±0.16 mechanical radian) both for EKF and HFI.

Looking at Fig. 9, one can notice that the Back-EMF exhibits poor results at standstill and at very low speed (these results were predictable as the electromotive forces vanish at low speed).

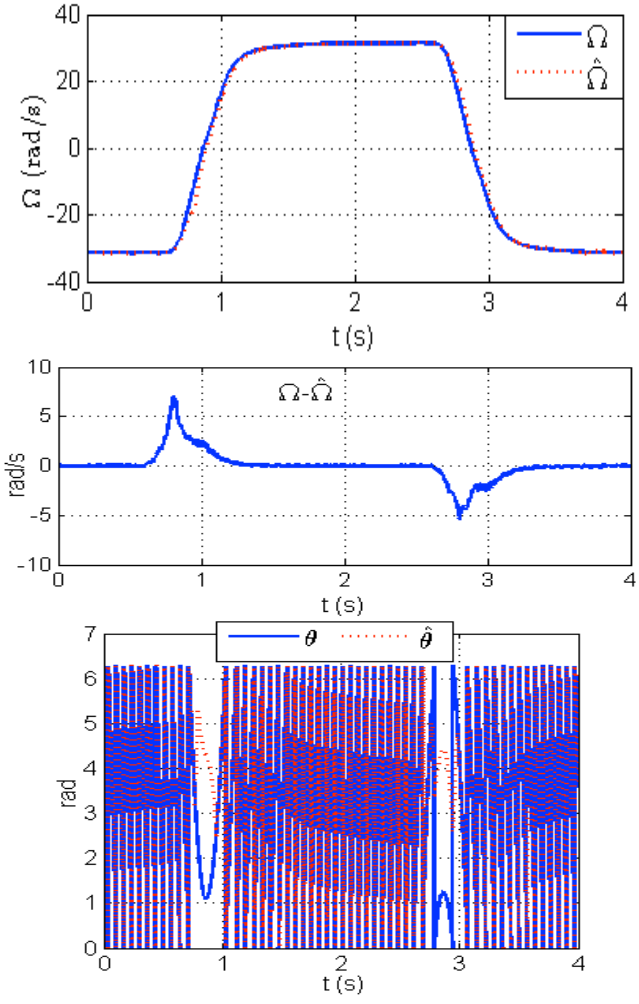

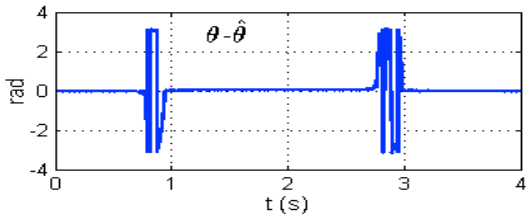

Fig. 9 – Back-EMF observer experimental results for speed and position estimations during a speed reversal test.

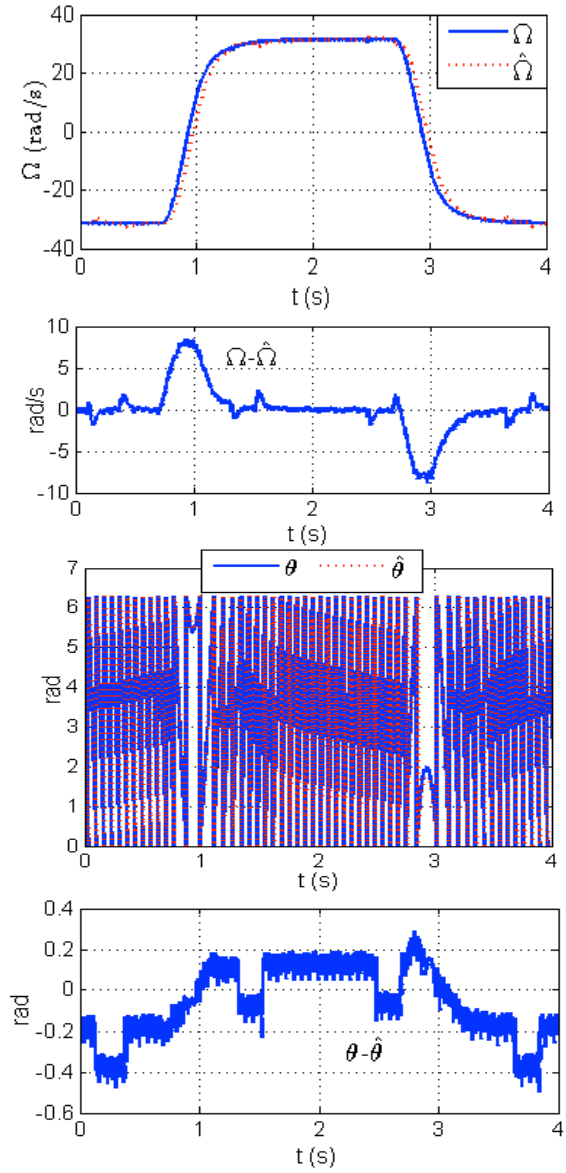

Fig. 10 – HFI sensorless experimental under speed reversal response.

The electrical position error estimation varies in the $\pm \pi$ radian at zero and very low speed operations during speed reversal. For the HFI estimator, in steady state, the position error is less than 0.1 rad while the speed error is almost zero.

These results show that in the low speed region, at position sensor fault occurrence, the drive would be more efficient if the estimated position is computed from the EKF or the HFI estimator.

The second operating point set at higher speed with a variable load torque (from 0 to 30 % of the nominal load torque between 0 and 0.5 s and between 3.5 and 5 s) has been selected to analyse the EKF and back-EMF performances. The results are displayed in Figs 11 and 12 respectively.

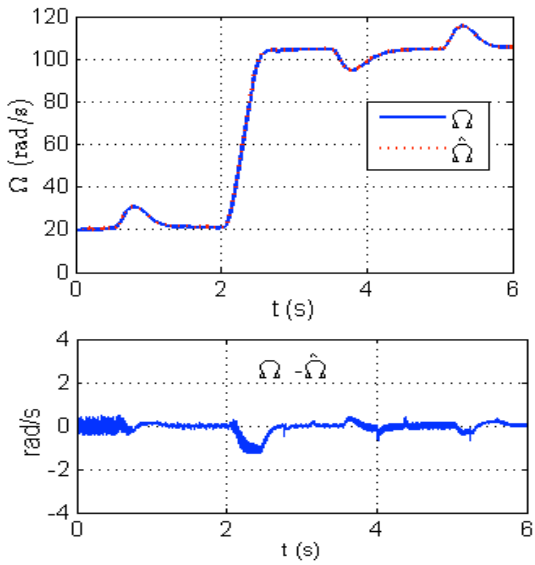

Fig. 11 – EKF Experimental results for speed estimation with a variable load torque.

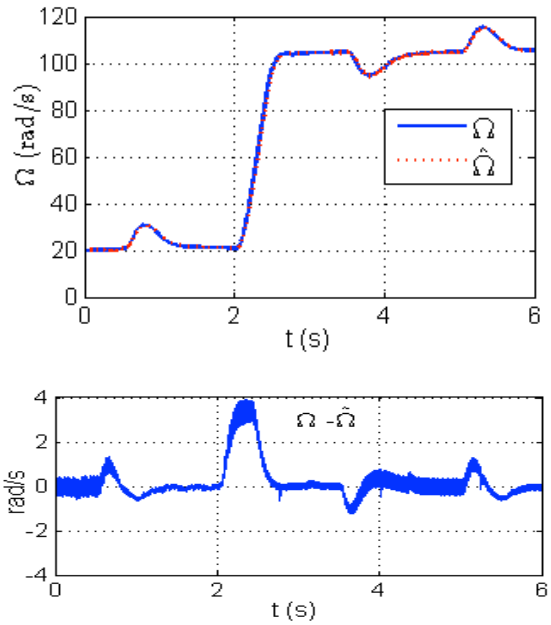

Fig. 12 – Back-EMF observer experimental results for speed estimation with a variable load torque.

The third operating mode is selected in sensorless control at low speed (around 10% of the nominal speed) with a variable load torque as in the second operating point.

The results displayed in Fig. 13 show the performances of the HFI when the load torque is variable. The average speed estimation error is almost zero and the position error mean value is around 0.25 rad.

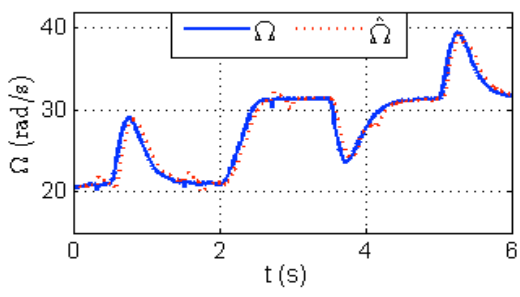

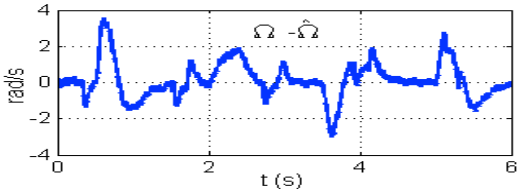

Fig. 13 – HFI experimental results for speed estimation with load torque variation.

4. CONCLUSIONS

This paper has presented a mechanical sensor fault tolerant controller for PMSM drives. At sensor fault occurrence, the drive enters in a sensorless mode in which the rotor position and speed must be estimated, as it is key information for the drive. We have evaluated on a test bench the performances of three estimators, the Extended Kalman Filter (EKF), the Back-EMF observer and the High Frequency Injection (HFI). The results show that at low speed (< 10%Ωn) including standstill, the EKF and the HFI are the estimators. For higher speeds, the EKF and the Back-EMF observer are the best candidates. Therefore, within the FTC, a supervision module is included to monitor continuously the mechanical sensor by comparing its output to the estimators in order to engage the best estimate at fault occurrence.

Received on June 13, 2019

REFERENCES

1. A. Khlaief, M. Boussak, M. Gossa, *Open phase faults detection in PMSM drives based on current signature analysis*, International Congress of Electrical Machines, Rome, 6–8, pp. 1–6, Sep. 2010.
2. M. Benbouzid, C. Delpha, Z. Khatir, S. Lefebvre, D. Diallo, *Faults detection and diagnosis in a static converter*", 2011, pp. 271-316, Electrical Machines Diagnosis, Trigeassou, J.C., Paris, Wiley, ISTE.
3. D. Diallo, M. Benbouzid, M.A Masrur; *Special Section on condition monitoring and fault accommodation in electric and hybrid propulsion systems*, IEEE Transactions on Vehicular Technology, **62**, *3*, pp. 962–964 (2013).
4. N. Layadi, A. Djerioui, S. Zeghlache, H. Mekki, A. Houari, M. Benkhoris, F. Berrabah, *New fault tolerant control based on backstepping controller for double star induction machine*, Rev. Roum. Sci. Techn. – Électrotechn. et Énerg., **64**, *3*, pp. 275–280, Bucarest (2019).
5. Y. Fan, W. Zhu, X. Zhang, M. Cheng, K. T. Chau, *research on a single phase-loss fault-tolerant control strategy for a new flux-modulated permanent-magnet compact in-wheel motor*, IEEE Trans. on Energy Conv. **31**, *2*, pp. 658-666, (2016).
6. E. Benyoussef, A. Meroufel, S. Barkat, "Neural network and fuzzy logic direct torque control of sensorless double star synchronous machine", Rev. Roum. Sci. Techn. – Électrotechn. et Énerg., **61**, *3*, pp. 239–243, Bucarest, 2016.
7. P.P. Vas, "Sensorless Vector and Direct Torque Control". London, U.K., Oxford Univ. Press, 1998.
8. C.S. Hsieh, F. C. Chen, *Optimal solution of the two-stage Kalman estimator*, IEEE Trans. Autom. Control, **44**, *1*, pp. 194–199 (1999).
9. Z. Chen, M. Tomita, S. Doki, S. Okuma, *An extended electromotive force model for sensorless control of interior permanent magnet synchronous motors*, IEEE Trans. Ind. Electron., **50**, *2*, pp. 288–295 (2003).
10. S. Diao, D. Diallo, Z. Makni, C. Marchand, J.F. Bisson, *A differential algebraic estimator for sensorless permanent-magnet synchronous machine drive*", IEEE Trans. on Energy conversion, **30**, *1*, pp. 82–89 (2015).
11. B. Belabbes, A. Larbaoui, *Commande passive associée à la commande par beckstepping d'un moteur synchrone*, Rev. Roum. Sci. Techn. – Électrotechn. et Énerg., **60**, *3*, p. 333–342 (2015).
12. A. Larbaoui, B. Belabbes, A. Meroufel, D. Bouguenna, *Commande par mode glissant floue de la machine synchrone*, Rev. Roum. Sci. Techn. – Électrotechn. et Énerg., **62**, *2*, pp. 192–196 (2017).
13. M. Hilairet, F. Auger, E. Berthelot, *Speed and rotor flux estimation of induction machines using a two-stage extended Kalman filter*, Automatica, **45**, *8*, pp. 1819–1827 (2009).
14. S. Bolognani, S. Calligaro, R. Petrella, M. Tursini, *Sensorless control of IPM motors in the low-speed range and at standstill by HF injection and DFT processing*, IEEE Trans. Ind. Appl., **47**, *1*, pp. 96–104 (2011).
15. Y. Yu, J. Tamura, D. D. Reigosa, R. D. Lorenz, *Position self-sensing evaluation of a FI-IPMSM based on high-frequency signal injection methods*, IEEE Trans. Ind. Appl., **49**, *2*, pp. 880–888 (2013).
16. J. Holtz, *Sensorless control of induction machines – with or without signal injection?* IEEE Trans. on Ind. Electronics., **53**, *1*, pp. 7-30 (2006).
17. M.S. Grewal, A. P. Andrews, *Kalman Filtering, Theory and Practice*, Englewood Cliffs, NJ, Prentice-Hall, 1993.
18. F. Auger et al., Industrial applications of the Kalman filter: a review, IEEE Trans. on Ind. Electronics, **60**, *12*, pp. 5458-5470 (2013).
19. Z. Boulbair, M. Hilairet, F. Auger, L. Loron, *Sensorless control of a PMSM using an efficient extended Kalman filter*, Int. Conf. of Electrical Machines ICEM04, Cracovia, Poland, 2004.
20. M. Shigeo, K. Keisuke, T. Yoji, *Position and speed sensorless control for IPMSM based on estimation of position error*, Electrical Engineers of Japan, **144**, *2*, pp. 722-729 (2003).
21. J. Lee, J. Hong, K. Nam, R. Ortega, L. Praly, A. Astolfi, Sensorless *control of surface-mount permanent magnet synchronous motors based on a nonlinear observer*, " IEEE Trans. on Power Electronics, **25**, *2*, pp. 290-297 (2010).
22. A. Sarikhani, O.A. Mohammed, *Sensorless control of PM synchronous machines by physics-based EMF observer*, IEEE Trans. Energy Convers., **27**, *4*, pp. 1009–1017 (2012).
23. Y.D. Yoon, S.K. Sul, S. Morimoto, K. Ide, *High-bandwidth sensorless algorithm for AD machines based on square-wave-type voltage injection*, IEEE Trans. Ind. Appl., **47**, *3*, pp. 1361–1370 (2011).
24. X. X. Luo, Q. Tang, A. Shen, Q. Zhang, *PMSM sensorless control by injecting HF pulsating carrier signal into estimated fixed-frequency rotating reference frame*, IEEE Trans. Ind. Electron., **63**, *4*, pp. 2294–2305 (2016).
25. C. Silva, G. M. Asher, M. Sumner, *Hybrid rotor position observer for wide speed-range sensorless PM motor drives including zero speed*, IEEE Trans. Ind. Electron., **53**, *2*, pp. 373–378 (2006).
26. M. W. Degne, R. D. Lorenz, *Using multiple saliencies of the estimation of flux, position, and velocity in AC machines*, IEEE Trans. Ind. Appl., **34**, *5*, pp. 1097–1104, (1998).
27. R. Isermann, *Fault-Diagnosis Systems: An Introduction from Fault Detection to Fault Tolerance*, Springer, 2006
28. D.R. Espinoza, D. U. Campos-Delgado, *Active fault tolerant scheme for variable speed drives under actuator and sensor faults*, Proc. IEEE Int. Conf. Control Appl., San Antonio, TX, USA, Sep. 2008, pp. 474–479.
29. J. Jiang, Xiang Yu, *Fault-tolerant control systems: A comparative study between active and passive approaches*", ISA Trans., Elsevier, **36**, pp. 60–72 (2012).
30. B. Tabbache, M. Benbouzid, A. Kheloui, J.M Bourgeot, Sensor *fault-tolerant control of an induction motor based electric vehicle*, European Conf. on Power Electroni and Applications, Aug. 2011.
31. M. Bourogaoui, H. BenAttia Sethom, I. S. Belkhodja, *Speed/position sensor fault tolerant control in adjustable speed drives – a review*, ISA Trans., Elsevier, **64**, pp. 269 –284 (2016).